Optimized Starbody Waverider Shapes for Lifting Aerocapture

Jeremy Knittel
University of Maryland
NASA Space Technology Research Fellow

Advisor Mark Lewis

9th International Planetary Probe Workshop
June 21, 2012

Agenda

- Motivation
- Starbody Fundamentals
- Trajectory Modeling
- Optimization Scheme
- Results
- Conclusions

Motivation

- Aerocapture is a promising means of increasing delivered payload mass
- Lifting aerocapture offers:
  - Decreased heat rate
  - *Increased heat load*
  - Decreased g-load
  - Increased entry corridor
  - Increased time of flight
- Starbody waveriders offer:
  - Low wave drag
  - Increased stability behavior

Starbody Waveriders

Nonweiler's Caret Wing

- Inversely designed from known compressible flow field
- Leading edges attached to shock plane

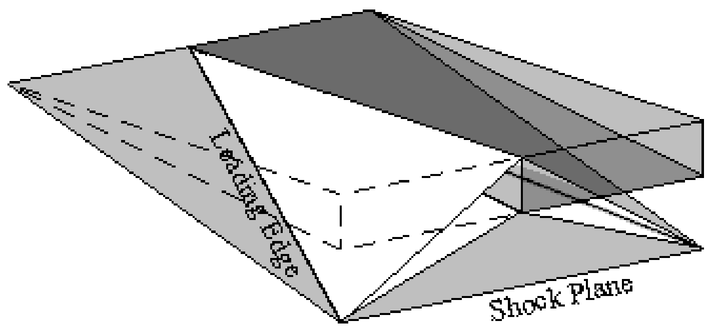

Reference: Nonweiler [5]

A. JAMES CLARK
SCHOOL OF ENGINEERING

Starbody Generation

- Attach multiple caret wings along leading edges
- Intersections of shock planes define leading edges
- Centerbody exposed to flow only at base of each caret wing

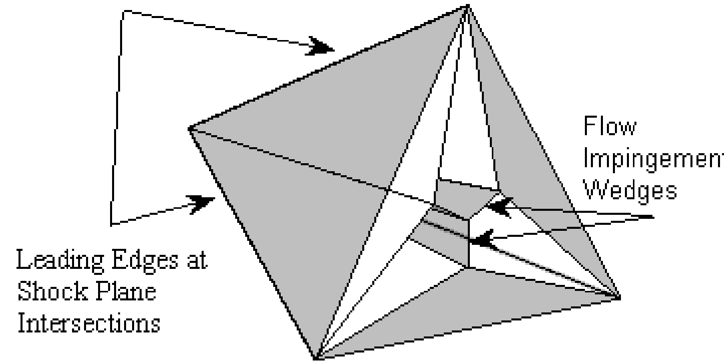

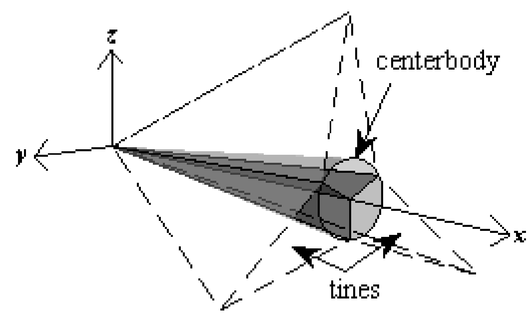

Starbody Generation

Steps for design a starbody

1. Using unit *l*, determine *R* from *l*/*R*.
2. Create centerbody ellipse (using *R* and *e*).
3. Determine locations around ellipse of flow disturbance
4. Calculate the resulting flow disturbance angle, θ, for each wedge.
5. Calculate shock-angle, β, using θ–β–M relation.
6. Find intersection lines of adjacent shock planes (these will be leading edges).
7. Connect all points to close vehicle

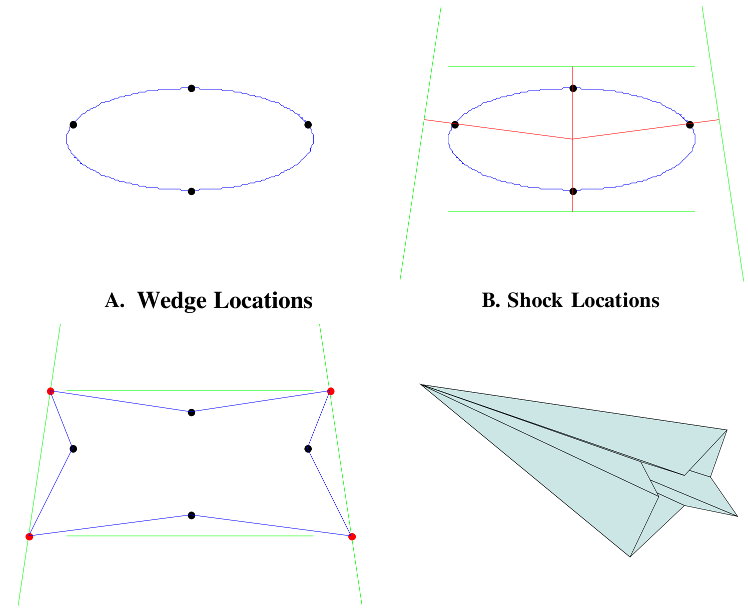

A. Wedge Locations

B. Shock Locations

C. Connect Shock Intersections with Wedge locations

D. 3d Model

A. JAMES CLARK SCHOOL OF ENGINEERING

Aerocapture Trajectory

Aerocapture Mission Profile

	High Energy Initial Orbit	Low Energy Initial Orbit
r_a	∞	∞
ε	20 km^2/s^2	12 km^2/s^2
v_∞	6.32 km/s	4.89 km/s
v_{entry}	~8 km/s	~7 km/s
γ_{entry}	~11°	~9°

- Mars selected as target planet due to higher fidelity models and high quality recent work
- Two entry scenarios created to compare effects of entry velocity
- To allow comparison to other recent work on Mars aerocapture, a heavy, 8000 kg entry mass vehicle was selected.

Wright, H., Oh, D., Westhelle, C., Fisher, J., Dyke, R., Edquist, K., Brown., J., Justh, H., Munk, M. ,"Mars Aerocapture Systems Study," NASA TM 2006-214522, August 2006.

Aerocapture Mission Profile

- The aerocapture was set to achieve a final orbit of 400 km altitude
- A target orbit was modeled which would allow the vehicle to travel from the edge of the atmosphere to the correct apoapsis point for a circularization burn

	Target Orbit	Final Orbit
h_a	400 km	400 km
h_p	< 50 km	400 km
ε	~(-5 km^2/s^2)	-5.64 km^2/s^2
e	$0 < e < 1$	0

UNIVERSITY OF MARYLAND 18 56

A. JAMES CLARK SCHOOL OF ENGINEERING

Control System

- Control system created to allow vehicle to modify its lift vector to reach desired target orbit
- Capable of being run at extremely high rate, appropriate for Monte Carlo/Optimization routines
- Simple algorithm based on altitude and energy triggers
- 3 triggers
  - Minimum altitude of negative lift, $h_{-\alpha}$
  - Maximum altitude of positive lift, $h_{+\alpha}$
  - Exiting energy

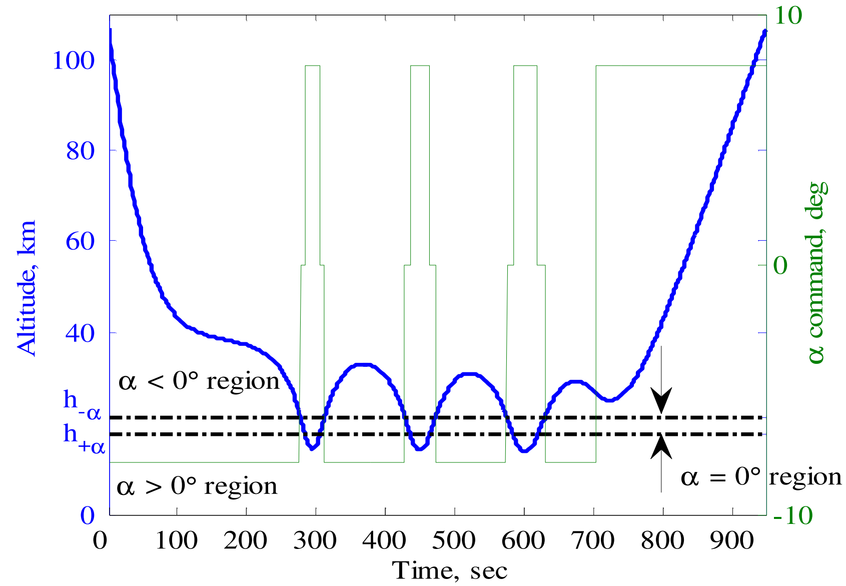

Optimization

Methodology

- Randomize sets of initial states within design space
  - Geometry Parameters
  - Control Triggers
  - Entry Flight Path Angle
- Use gradient based routine to minimizes objective function
- Combined Monte Carlo and Gradient Optimizer!
- Denominator ensures proper amount of energy dissipation occurs
- Numerator decreases average energy dissipation rate without biasing towards a specific dissipation path

$$F = \frac{-(t_{exit} - t_{entry})}{\left|(\varepsilon_f - \varepsilon_T)\right|}$$

Results

Trajectory Types

- Skipping
  - Phased deceleration
  - Number and altitude amplitude of skips varies
- Single Skip
  - Non-lifting trajectory
  - High g-loads
  - High heating rates
- Altitude Hold
  - High lifting
  - Requires high levels of control

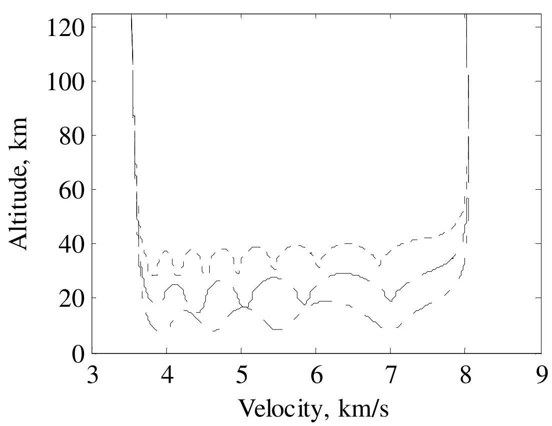

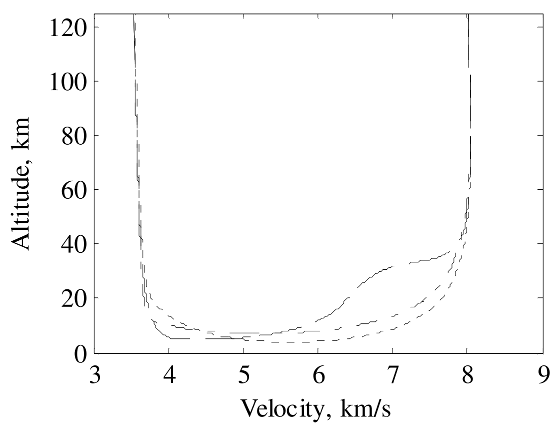

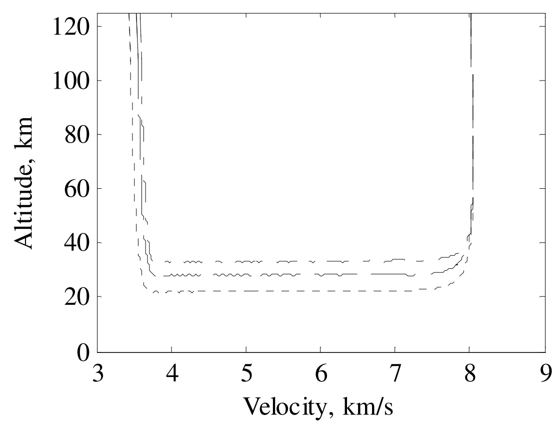

Effects of Entry Velocity

- High heat load trajectories favored
  - Inevitable with lifting trajectories
  - Objective function favored high heat load
- Consistency of Mach range supports use of waveriders for aerocapture trajectories

Heat Rate vs. Heat Load Tradeoff

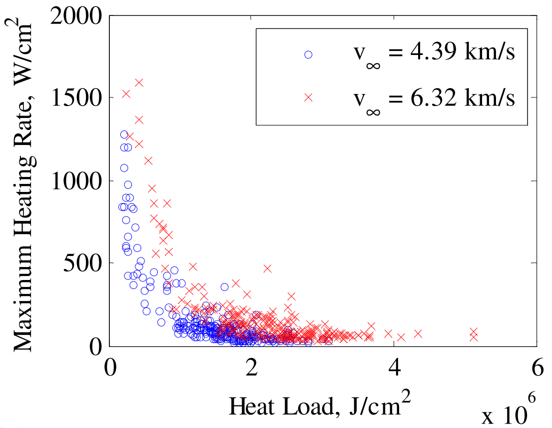

Mach Number during Peak Dynamic Pressure

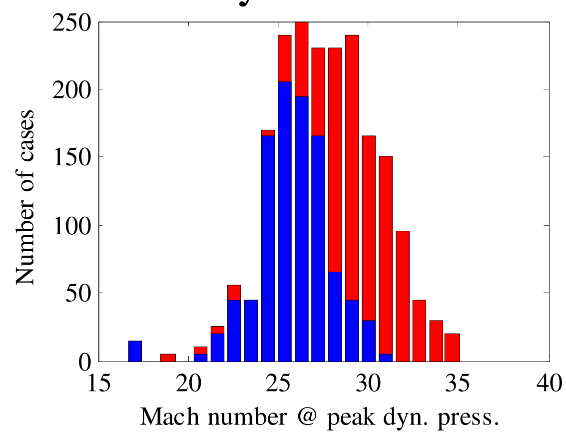

A. JAMES CLARK
SCHOOL OF ENGINEERING

Geometric Effects

- L/D ~ 2 is frequently optimal!
- L/D > 3 is rarely optimal!
- Trend in g-load is independent of tine number: No reason to select less volumetrically efficient tine number designs!

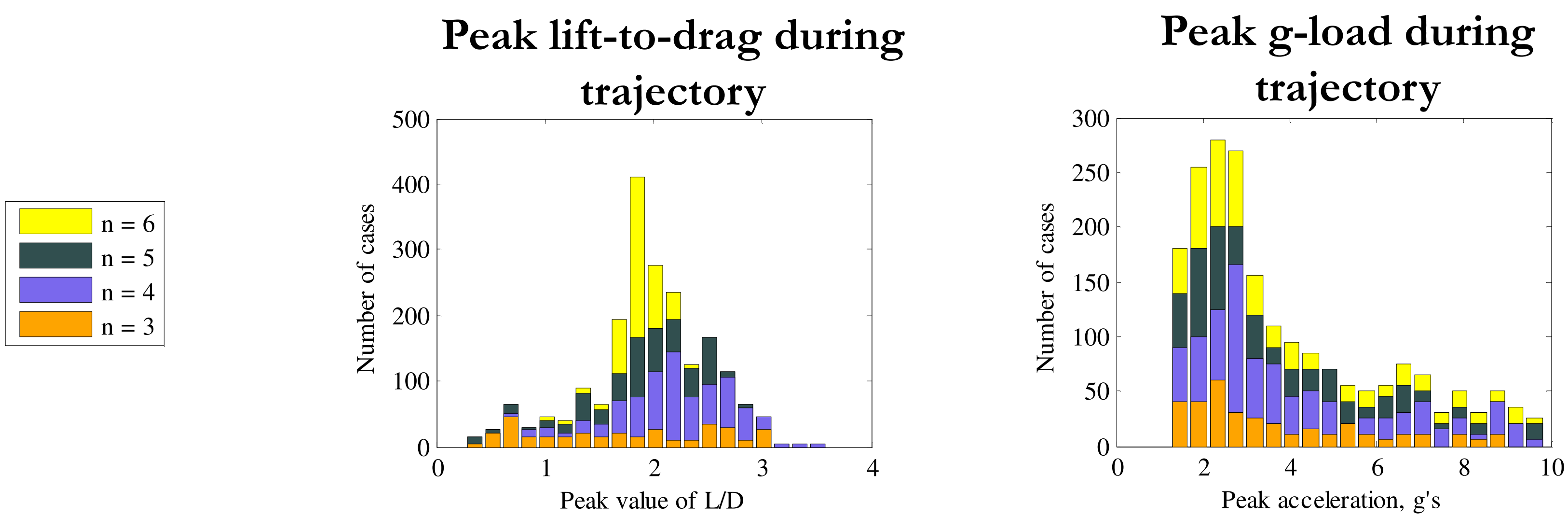

UNIVERSITY OF MARYLAND 18 56

A. JAMES CLARK SCHOOL OF ENGINEERING

NASA

Entry Corridors

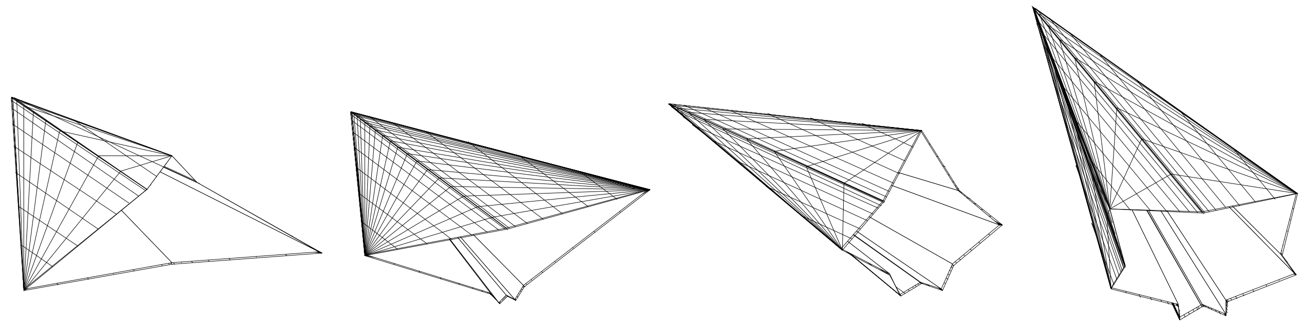

	n	3	4	5	6
	γ_+	-9.11°	-8.90°	-9.73°	-9.79°
v_∞= 6.32 km/s	γ_-	-14.14°	-15.24°	-15.24°	-14.73°
	Corridor	**5.03°**	**6.34°**	**5.51°**	**4.95°**
	γ_+	-8.95°	-8.90°	-9.25°	-9.32°
v_∞= 4.89 km/s	γ_-	-14.15°	-13.64°	-14.64°	-14.65°
	Corridor	**5.20°**	**4.74°**	**5.39°**	**5.27°**

Conclusions

Conclusions

- Novel starbody waverider parameterization presented
- A simple control model can accurately analyze the aerocapture problem
- Peak near L/D = 2 is worth further investigation
- Extreme lifting (max L/D > 3) is not necessary or optimal
- Consistency of Mach range at peak dynamic pressure supports use of waveriders for aerocapture trajectories
- Entry corridors are extremely large for lifting bodies
- Future Work
  - An aerothermal model is necessary to further analyze the overall heat load
  - More specific objective function associated with specific mission
  - Other aero-assisted trajectories:
    - Aerogravity Assist
    - Plane Change
    - Steady, atmospheric perigee orbital flight

Questions

Aerodynamic Forces

- Vehicle is comprised of $2n$ flat surfaces
- Pressure force calculation from oblique shock theory
- Viscous forces
  - Proportional to distance from leading edge
  - Requires double integration due to swept leading edge
- Coefficients calculated as summation over all $2n$ surfaces

$$F_P = P_2 \frac{bL}{2}$$

$$F_\tau = \frac{25}{18} \tau^* \frac{bL^{.8}}{2} cos^{.2}(\theta)$$

$$C_D = \frac{1}{\frac{1}{2}\rho_\infty v^2 S} \left\{ \sum_m^{2*n} F_P(\hat{n}_m \cdot \hat{x}) - \sum_m^{2*n} F_\tau(\hat{t}_m \cdot \hat{x}) \right\}$$

$$C_L = \frac{1}{\frac{1}{2}\rho_\infty v^2 S} \left\{ \sum_m^{2*n} F_P(\hat{n}_m \cdot \hat{z}) - \sum_m^{2*n} F_\tau(\hat{t}_m \cdot \hat{z}) \right\}$$

Reference: Tarpley [9]

UNIVERSITY OF MARYLAND 18 56

A. JAMES CLARK SCHOOL OF ENGINEERING

NASA

Off-Design Conditions

- Two categories of conditions:
  - Below design
    - Pitch towards shock plane
    - Flight M decreases
  - Above design
    - Pitch away from shock plane
    - Flight M increases
- Under strong shock condition, pressure decreases towards centerbody
- Under weak shock condition, pressure increases towards centerbody

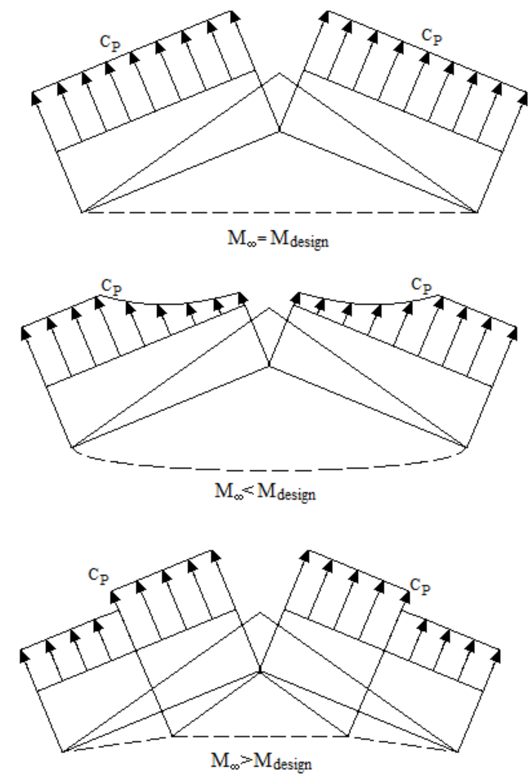

Reference: Tarpley [9]

Equation of Motion

- 3 DOF simulation
- Aerodynamic forces added to gravitational forces and resolved into planet centered inertial frame
- Equation in the *i*-direction:

$$a_i = -\frac{\mu}{r^3} r_i + \frac{1}{2}\rho_\infty v^2 \frac{S}{m}\left(\frac{r_i}{r} C_L - \frac{v_i}{v} C_D\right)$$

Design Space

- 3 geometry variables
  - Number of tines, *n*
  - Tine distribution parameter, *D*
  - Centerbody eccentricity, *e*
- 6 trajectory variables
  - Radius of perigee (1)
    - If there were no atmosphere
    - Effectively varies entry flight path angle
  - Control system triggers
    - Min. altitude of negative lift (2)
    - Max. altitude of positive lift (3)
    - Exiting energy (4)
  - Angle of attack in each region (5,6)

	Min	**Max**
D	-1	1
e	-1	1
γ_{entry}	-16°	-8°
$h_{-\alpha}$	$h_{+\alpha}$	55 km
$h_{+\alpha}$	0 km	$h_{-\alpha}$
α_{+}	0°	8°
α_{-}	-8°	0°
ε_{ascent}	-5 km^2/s^2	-3 km^2/s^2

A. JAMES CLARK SCHOOL OF ENGINEERING

Monte Carlo Simulation

- Main Run
  - 4000 cases of randomized initial inputs
  - 2931 cases found locally optimal solutions
  - 2020 cases reached within 1% of the targeted energy, flight path angle and velocity at exit
- Fixed Geometry study
  - Used to study the most locally optimal geometries from the main run
  - 1600 cases of randomized trajectory inputs
  - 1435 cases found locally optimal solutions
  - 923 cases reached within 1% of the targeted energy, flight path angle and velocity at exit

Volumetric Efficiency

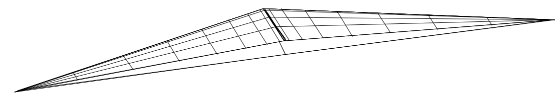

- Representation of usable volume
- Scaled to give spheres 100% efficiency
- 3,4 tine starbodies have low and η_v peaks
  - Lower peak corresponds to high aspect ratio designs with very high lift
  - Higher peak corresponds to more blunt designs. Less lift implies need for greater drag to complete aerocapture
- 5,6 tine starbodies inherently more efficient
  - Increased number of tines prevents high aspect ratio designs
  - High volume does not necessarily imply non-lifting designs

$$\eta_V = \frac{(36\pi)^{1/3} V^{2/3}}{S}$$

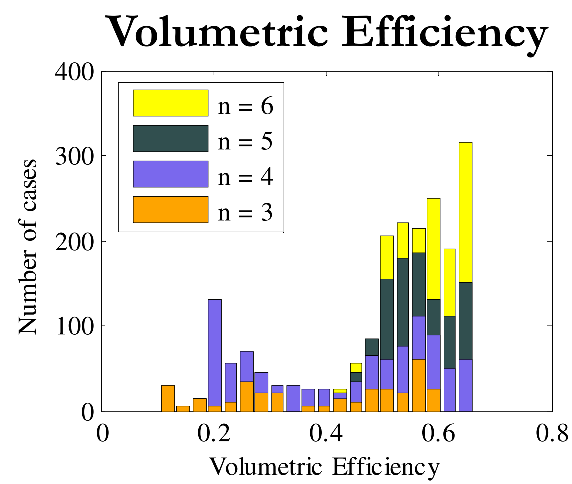

Reference: Johnson [11]

UNIVERSITY OF MARYLAND 1856

A. JAMES CLARK SCHOOL OF ENGINEERING

Trajectory Types

- Due to solution scheme:
  - Skipping methods most frequent
  - Altitude hold is somewhat common
  - Single skip trajectories are infrequent
    - Starbodies have insufficient wave drag
    - Objective function favored longer time of flight
- Control scheme had high degree of success in reaching 400 km apoapsis
  - Skipping methods reached target less frequently percentagewise
    - Control system limitations
    - Inaccuracies were almost all undershoot
  - Almost all single skip trajectories reached target

Time of Flight

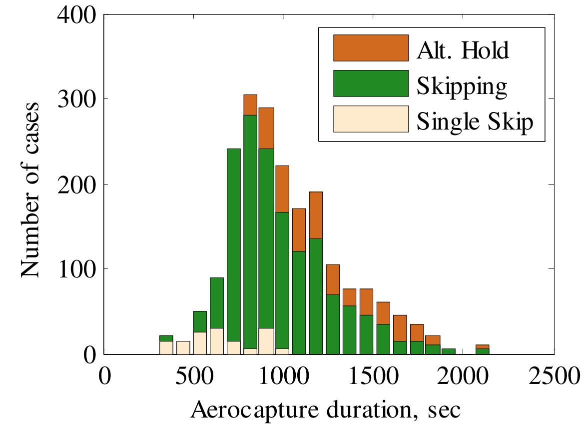

Altitude of Apoapsis

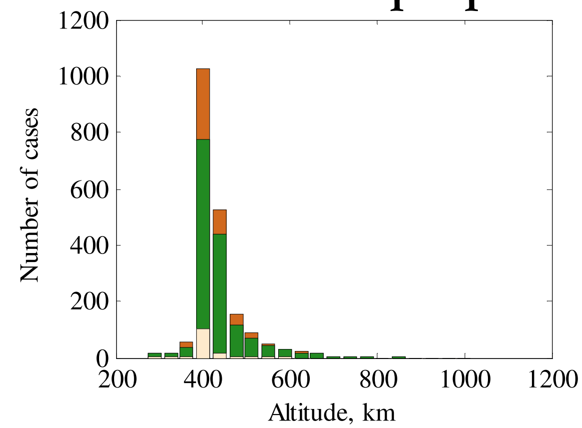

"Optimal" Designs

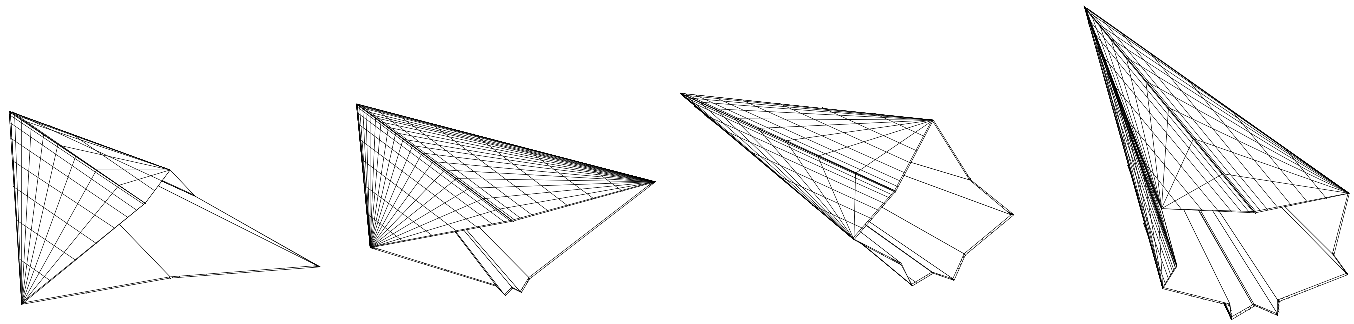

n	3	4	5	6
V	40 m^3	40 m^3	40 m^3	40 m^3
m	8000 kg	8000 kg	8000 kg	8000 kg
D	.380	-.724	-.442	.616
e	-.223	-.625	.031	-.742
l	11.0 m	9.8 m	11.7 m	13.9 m
$\mathbf{b_{max}}$	4.15 m	4.35 m	1.82 m	1.78 m
S	103.2 m^2	109.83 m^2	87.3 m^2	92.27 m^2
η_V	54.8 %	51.5 %	64.4 %	61.3%
Max L/D	2.48	2.97	1.98	2.17

References

1. Anderson, J., Lewis, M., Kothari, A., and Corda, S. "Hypersonic Waveriders for Planetary Atmospheres," *Journal of Spacecraft,* Vol. 28, pp 401-410, 1991.
2. Lewis, M. "The Use of Hypersonic Waveriders for Aero-assisted Manouevring," *Journal of the British Interplanetary Society,* Vol. 46, pp 11-20, 1993.
3. Hui, W. "Stability of Oscillating Wedges and Caret Wings in Hypersonic and Supersonic Flows," *AIAA Journal*, Vol. 7, pp 1524-1530, 1969.
4. Tarpley, C., Lewis, M. "Stability and Control of for a Hyperonic Caret-Wing Waverider," *Journal of Aircraft*, Vol. 32, pp 795-803, 1995.
5. Nonweiler, T. "Aerodynamic Problems of Manned Space Vehicles," *Journal of the Royal Aeronautical Society,* Vol. 63, pp 521-528, 1959.
6. Mascitti, V. "A Closed-form Solution to Oblique Shockwave Properties," *Journal of Aircraft,* Vol. 6, pp 66-78, 1969.
7. Wright, H., Oh, D., Westhelle, C., Fisher, J., Dyke, R., Edquist, K., Brown., J., Justh, H., Munk, M. "Mars Aerocapture Systems Study," NASA TM 2006-214522, August 2006.
8. Korzun, A., Dubos, G., Iwata, C., Stahl, B., Quicksall., J. "A Concept for the Entry, Descent, and Landing of High-Mass Payloads at Mars." *Acta Astronautica*, Vol. 66, pp 1146-1159, 2010.
9. Tarpley, C. "The Optimization of Engine-Integrated Hypersonic Waveriders with Steady State Flight and Static Margin Constraints," *PhD Thesis, University of Maryland, College Park*, 1995.
10. Regan, F., Anandakrishnan, S. *Dynamics of Atmospheric Re-entry.* AIAA education series, 1993.
11. Johnson, J. "Aerothermodynamic Optimization of Earth Entry Blunt Body Heat Shields for Lunar and Mass Return," *PhD Thesis, University of Maryland, College Park*, 2009.